Surv Geophys (2015) 36:549–570
DOI 10.1007/s10712-015-9327-1

Seismic *b*-Values, Bouguer Gravity and Heat Flow Data Beneath Eastern Anatolia, Turkey: Tectonic Implications

Nafiz Maden[1] · **Serkan Öztürk**[1]

Received: 17 November 2014 / Accepted: 8 April 2015 / Published online: 29 April 2015

Abstract In this paper, we analyze the relationships between the seismic *b*-values, Bouguer gravity and heat flow data in the Eastern Anatolia region of Turkey. For this purpose, spatial distributions of *b*-value, Bouguer gravity and heat flow have been presented for different depths and locations. In distinction to previous studies which have used only two parameters (gravity and seismic *b*-value or heat flow and seismic *b*-value), we have combined seismic *b*-values, Bouguer gravity and heat flow data to determine the new results on the active tectonics of the Eastern Anatolia region. Our analysis shows that there are significant and robust correlations amidst the heat flow data, Bouguer gravity anomaly and seismic *b*-values. The crustal structure is thick in areas where the large negative gravity anomalies and low *b*-values are observed. On the contrary, the regions with positive gravity anomalies and high *b*-values are likely to be associated with magma chambers or crustal low-velocity zones. We also provide some evidence suggesting that high *b*-values and high heat flow values can be related to the magmatic activities beneath the volcanic chain in the Eastern Pontide orogenic belt. Consequently, we have reached some conclusions for the Eastern Anatolia region: (1) The Moho to surface is rather thick and earthquakes are relatively smaller beneath the volcanic chain where the high heat flow values are observed, (2) a southward subduction model could have existed for the development of the Pontides during the late Mesozoic–Cenozoic era, (3) hot and unstable mantle lid zones or a lithosphere deprived of mantle under the study region is much more plausible, (4) a southward movement of the subduction plate and a northward extension of the Black Sea increase the state of stress along the trench axis and decrease the *b*-value, and (5) these movements may load the stress energy to the fault zones, thereby causing the catastrophic earthquakes in the Eastern Anatolia region.

Keywords Seismic *b*-values · Gravity anomalies · Heat flow · Subduction · Tectonic implications · Eastern Anatolia

✉ Nafiz Maden
nmaden@gumushane.edu.tr

[1] Department of Geophysics, Gümüşhane University, 29100 Gümüşhane, Turkey

1 Introduction

It is widely accepted that the *b*-value is quite an important seismic parameter related to the tectonic and thermal properties, material heterogeneity and ductility of the rocks for a given region (Aki 1965; Wiemer et al. 1998; Olsson 1999; Bayrak and Özturk 2004; Öztürk et al. 2008; Öztürk 2011). However, the correlation between seismic *b*-value and gravity anomaly or between seismic *b*-value and heat flow data for different parts of the world has not been studied intensively. Previous studies, which have dealt with the tectonic implications (TIs), have concentrated only on two parameters: either *b*-value with Bouguer anomaly or *b*-value with heat flow data (Wang 1988; Khan 2005; Khan and Chakraborty 2007; Sobiesiak et al. 2007; Kalyoncuoglu et al. 2011, 2013). Khan and Chakraborty (2007) attempted a multivariate analysis for the Shillong Plateau with an excellent correlation between the seismic *b*-value and the Bouguer gravity data. Sobiesiak et al. (2007) used the spatial *b*-value distribution and isostatic residual gravity anomalies to identify the asperity structures in the north Chilean subduction zone.

There are very few studies between *b*-values, Bouguer anomaly, heat flow and TI for different parts of the Turkey. Kalyoncuoglu et al. (2011) suggested the presence of a northward subduction zone beneath Anatolia in the Antalya Bay extending from the western part of the Cyprian arc to the Isparta Angle by using the seismic *b*-values and gravity data. Recently, Kalyoncuoglu et al. (2013) analyzed the spatial distribution of earthquakes, *b*-value and heat flow data to reveal the deep structural features of the Aegean region. In this study, we try to answer the following question: "How can the regional distributions of seismic *b*-value, Bouguer anomaly and heat flow parameters be evaluated as an important tectonic tool?" More specifically, what kind of analysis must be made to understand the correlations between the TI model and the parameters mentioned above? Which can be evaluated in relation to crustal setting and stress regime of the study area?

b-Value is estimated from the Gutenberg–Richter relation (Gutenberg and Richter 1944), and it is one of the best known empirical relations in seismology. *b*-Value, which gives an estimate of the slope or the magnitude–frequency distribution of earthquakes, is one of the most important indicator parameters of the rheological and geotectonic features of the Earth's materials (Déverchère et al. 2001; Fagereng 2001; Kalyoncuoglu et al. 2013). Seismic tomography, heat flow and gravity studies are capable of identifying the crustal or upper mantle heterogeneity, but fail to account for the stress levels associated with these features (Khan and Chakraborty 2007). Fluctuations in *b*-value from its average value of about 1 may result from various reasons. Increased crack density or material heterogeneity results in large *b*-values (Mogi 1962), while an increase in the shear stress or decrease in the confining pressure (Scholz 1968; Wyss 1973) decreases the *b*-value. Also, the *b*-values can be related to the plate subduction rate (Cao and Gao 2002), and thus, an increase in plate subduction rate may lead to an increase in volcanic activity. The *b*-value may also be related to both gravity anomaly and heat flow data. For example, the steeply dipping gravity anomaly usually results in a low *b*-value (Wang 1988).

The Eastern Anatolia region (Fig. 1), where many large earthquakes have occurred, especially in the last 10 years, is one of the geologically most complex, intensely deformed and continent–continent collision areas within the Alpine–Himalayan system (Şengör and Kidd 1979; Şengör et al. 1985; Yılmaz et al. 1987; Pearce et al. 1990). This region has also many important tectonic systems such as the East Anatolian Fault Zone, Dead Sea Transform Fault Zone, Bitlis Thrust Zone and Karlıova triple junction, which play an important role in the assessment of the TI. Also, the subduction polarity, which is liable for

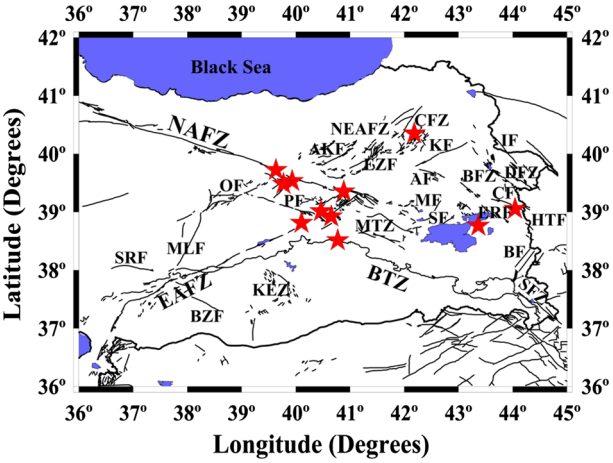

Fig. 1 Simplified tectonic map illustrating major faults in the Eastern Anatolia region. Tectonic structures were modified from those given by Şaroğlu et al. (1992), Bozkurt (2001) and Ulusay et al. (2004). Some large earthquakes mentioned in the text (in Sect. 2) are shown with stars. (Names of faults: *NAFZ* North Anatolian Fault Zone, *EAFZ* East Anatolian Fault Zone, *BTZ* Bitlis Thrust Zone, *NEAFZ* North East Anatolian Fault Zone, *ÇFZ* Çobandede Fault Zone, *AKF* Aşkale fault, *EZF* Erzurum fault, *KF* Kağızman fault, *AF* Ağrı fault, *IF* Iğdır fault, *DFZ* Doğubeyazıt Fault Zone, *BFZ* Balıklıgölü Fault Zone, *ÇF* Çaldıran fault, *ERF* Erciş fault, *HTF* Hasan-Timur Fault, *BF* Başkale fault, *YSFZ* Yüksekova-Şemdinli Fault Zone, *SF* Süphan fault, *MF* Malazgirt fault, *MTZ* Muş Thrust Zone, *KEZ* Karacadağ Extension Zone, *BZF* Bozova fault, *SRF* Sürgü fault, *MLF* Malatya fault, *OF* Ovacık fault, *PF* Pülümür fault)

the development of the Pontides, is still under debate due to the limited geological, geophysical and geochemical data sets that are available.

This study attempts to identify the key stages of the geological processes and to answer the questions posed above for a detailed assessment about TI. In this research, our main purpose is to analyze the relations between *b*-values, gravity anomaly and heat flow data in the Eastern Anatolia region. These relations are important in order to interpret the TI in a more meaningful way and to better understand the plate movements which depend on the stress regime of the crust in the study region. Thus, this study focuses on the comparison of: (1) regional distribution of *b*-value as a function of depth, (2) Bouguer gravity and (3) heat flow maps. Consequently, this research contributes to the understanding of low-velocity zones beneath the East Anatolian plateau (Al-Lazki et al. 2004) that could be a result of the subducted Tethyan oceanic lithosphere.

2 Tectonic Settings

The study region is limited by the coordinates 36°N and 42°N in latitude and 36°E and 45°E in longitude since many large earthquakes have occurred in this region since the year 2000. A map of the active fault systems of the eastern part of Turkey shown in Fig. 1 is based on the maps of different authors such as Şaroğlu et al. (1992), Bozkurt (2001) and Ulusay et al. (2004).

The East Anatolian Fault Zone (EAFZ) is a 550-km-long (Fig. 1), approximately northeast-trending, sinistral strike-slip fault zone that comprises a series of faults arranged parallel, subparallel or obliquely to the general trend. This fault zone is a transform fault

forming parts of boundaries between the Eurasian and the Anatolian plates and between the African and Arabian plates (Westeway 1994). It is considered as a conjugate structure to the North Anatolian Fault Zone (NAFZ). The EAFZ extends from Karlıova in the northeast to Kahramanmaraş, an area in the southwest, where it meets and forms triple junctions with the NAFZ and the Dead Sea Fault Zone (DSFZ), respectively (Bozkurt 2001).

The Dead Sea Transform Fault Zone (DSTFZ) is a 1000-km-long, approximately N–S trending, sinistral intraplate strike-slip fault zone. In terms of plate tectonics, the DSFZ is considered to be a plate boundary of the transform type, separating the Arabian Plate to the east from the African Plate to the west (Şengör and Yılmaz 1981). The Arabian Plate is moving northward faster than the African Plate. This differential movement between these plates is taken up by the DSFZ. Tectonically, the DSFZ joins the divergent plate boundary along the Red Sea with the zone of plate convergence along the Alpine–Himalayan belt in southern Turkey (Hempton 1987). The DSFZ and the EAFZ meet at a triple junction between the African, Anatolian and Arabian plates near Kahramanmaraş.

The Arabian and Eurasian plates collide along the Bitlis Thrust Zone (BTZ) (Fig. 1), resulting in the uplift of mountains along the suture. The BTZ is a complex continent–continent and continent–ocean collisional boundary that lies north of the fold-and-thrust belt of the Arabian platform and extends from southeastern Turkey to the Zagros Mountains in Iran (Şengör and Yılmaz 1981).

The area to the east of the Karlıova triple junction is characterized by a north–south compressional tectonic regime. Conjugate strike-slip faults of dextral and sinistral character paralleling the North and East Anatolian Fault Zones dominate the region (Bozkurt 2001). These structures include many faults such as the Çaldıran Fault, Erciş Fault, Iğdır Fault, Malazgirt Fault, Süphan Fault, Kağızman Fault Zone, Tutak Fault Zone and North East Anatolian Fault Zone (Fig. 1). Although the conjugate strike-slip fault system dominates the active tectonics of Eastern Anatolia, the east–west trending basins of compressional origin form the most spectacular structures of the region as they indicate north–south convergence and a shortening of the Anatolian plateau (Wong et al. 1978).

3 Data and Methods

The earthquake database used in this analysis is taken from Öztürk (2009) for the time period between 1970 and 2006. He prepared an instrumental earthquake database for duration magnitude, M_D. This seismicity catalogue from 1970 to 2006 consists of 6457 events (depths less than 70 km) whose magnitudes are equal to and larger than 1.8 on the Richter scale. In this study, we used the Kandilli Observatory and Research Institute (KOERI) catalogue, Bogazici University, for the period between 2006 and 2014. KOERI has computed the size of all earthquakes with M_D and provides the real time data with the modern online and dial-up seismic stations in Turkey, especially after 2000. In recent years, KOERI supplies local magnitude, M_L, with the local stations with missing M_D magnitudes. If M_D is unknown in the KOERI catalogue for the time interval between 2006 and 2014, M_D values were computed from the M_D–M_L relationships of Öztürk (2009).

Thus, we have 24,004 earthquakes with magnitudes $M_D \geq 1.0$ for the eastern part of Turkey between 2006 and 2014. The time interval is from April 21, 1970, to December 31, 2013, which is about 43.7 years, and the database for the eastern part of Turkey includes in total 30,461 earthquakes between 1970 and 2014. The depths of the earthquakes are less than 70 km, and the magnitudes for all events are between 1.0 and 6.6. The epicenter

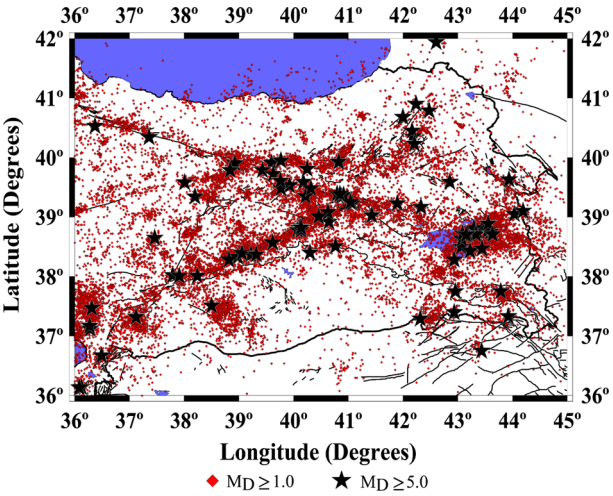

Fig. 2 Epicenter distributions of all earthquakes with $M_D \geq 1.0$ and depth <70 km in the Eastern Anatolia region between February 1970 and December 2013. *Stars* represent the principal main shocks with $M_D \geq 5.0$

distributions of all earthquakes and the principal main shocks ($M_D \geq 5.0$) are shown in Fig. 2.

The Bouguer gravity data of the study region, which is gridded at an interval of 2.5 km, are taken from the General Directorate of Mineral Research and Exploration (MTA). Bouguer gravity values are connected to MTA and General Command of Mapping base stations related to the Potsdam absolute gravity value 981,260.00 mGal acknowledged by the International Union of Geodesy and Geophysics in 1971. A latitude correction was used according to the Gravity Formulae of 1967. Bouguer reduction was applied for a density of 2.40 Mg m^{-3}. Topographic correction was determined up to a distance of 167 km, considering a terrain density of 2.67 Mg m^{-3}.

Tezcan and Turgay (1989) produced preliminary heat flow maps for Turkey by determining geothermal gradients with a constant thermal conductivity values in exploration wells. A new heat flow map for Turkey was determined by İlkışık (1992) from silica contents from chemical analyses of thermal springs. According to İlkışık (1992), the average heat flow value is 110.7 mW m^{-2} in Western Anatolia, 102.8 mW m^{-2} in Central Anatolia, and 112.8 mW m^{-2} in Eastern Anatolia. Tezcan (1995) updated the first heat flow map of Tezcan and Turgay (1989) by using temperatures measured in 204 oil and coal wells mostly drilled in southeastern Turkey and the Thrace Basin. It was stated that the heat flow values over Anatolia are much higher than those over the Mediterranean and the Black Sea (Tezcan 1995). The highest heat flow value of 247 mW m^{-2} from silica content analysis was achieved near Gediz Valley (İlkışık 1995). In the Ihlara Valley, İlkışık et al. (1997) obtained the average heat flow value by using both silica and gradient techniques as 158.5 mW m^{-2}.

3.1 *b*-Value of Gutenberg–Richter (Magnitude–Frequency) Relation and Completeness Magnitude (Mc)

In the present study, an effort is made to analyze the correlations between the regional distribution of seismic *b*-values with Bouguer gravity anomaly and with heat flow

distribution over the whole Eastern Anatolia region. Shallow earthquakes (<70 km) are selected to analyze the seismicity since the seismogenic layer is suggested to be only 40–50 km thick for the eastern part of Turkey (Gök et al. 2007).

The size distribution of earthquakes in most cases is well described by the Gutenberg and Richter (1944) relationship:

$$\log_{10} N(M) = a - bM \tag{1}$$

where $N(M)$ is the cumulative number of earthquakes with magnitudes equal to or larger than M, b describes the slope of the size distribution of events, and a is proportional to the productivity of a volume or the seismicity rate. Although a-values and b-values are determined empirically from seismic catalogues, it is imperative to understand their physical meaning. Estimates of b-value imply a fractal relation between frequency of occurrence and the radiated energy, seismic moment or fault length, and this is one of the most widely used statistical parameters to describe the size scaling properties of seismicity. Utsu (1971) summarized that b-values change roughly in the range from 0.3 to 2.0, depending on the region. However, on average, the regional-scale estimates of b-value are approximately equal to 1 (Frohlich and Davis 1993). The maximum-likelihood method provides the least-biased estimate of b-value (Aki 1965):

$$b = 2.303/(M_{\text{mean}} - M_{\text{min}} + 0.05) \tag{2}$$

where M_{mean} is the mean magnitude of events and M_{min} is the minimum magnitude of completeness in the earthquake catalogue. Accurate estimates of local changes of M_{min} can be made if relatively large numbers (100 or so) of local observations are available for analysis (Wiemer and Wyss 2000). The value 0.05 in Eq. (2) is a correction constant that compensates for rounding errors. The 95 % confidence limits on the estimates of b-value are $\pm 1.96b/\sqrt{n}$, where n is the number of earthquakes. This yields confidence limits of ± 0.1–0.2 with a typical value of $n = 100$ earthquakes.

The completeness magnitude, above which all events have been recorded, is important for all seismicity-based studies because it is appropriate to use the maximum number of events available for high-quality results. The estimation of the completeness magnitude (Mc) is based on the assumption that the earthquakes obey the Gutenberg–Richter's power law (Wiemer and Wyss 2000). The completeness magnitude varies as a function of space and time, so particularly the temporal changes can potentially produce erroneous estimates of seismicity parameters, especially the b-value. Because the temporary stations may be installed after the main shock and during the first highest activity, small shocks may not be spatially located since they fall within the coda of larger events; Mc will be higher in the early part of the earthquake catalogue (Wiemer and Katsumata 1999). Since a part of this study deals with the spatial variation of b-value and not of energy or moment release, the completeness magnitude of used events for estimating the b-value distribution is important because the Mc changes regionally depending on the seismic activity and the sensitivity of the stations.

4 Results and Discussion

The relationships between seismic b-value, Bouguer gravity anomaly and heat flow behaviors in the eastern part of Turkey are studied by imaging the spatial variations of these parameters. The slope of the frequency–magnitude distribution is given by the Gutenberg–

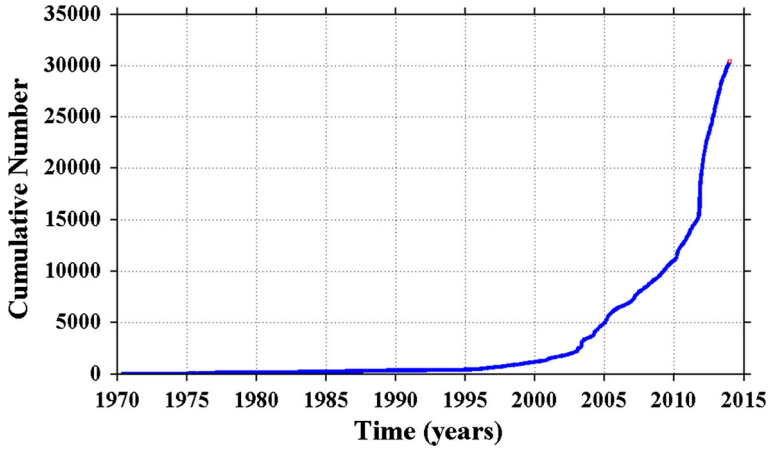

Fig. 3 Cumulative number of earthquakes for the time period 1970–2014 in the Eastern Anatolia region

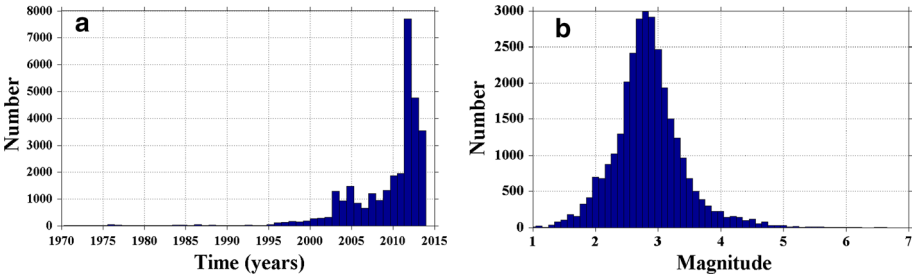

Fig. 4 Time (**a**) and magnitude histograms (**b**) of the earthquakes for the time period 1970–2014 for the Eastern Anatolia region

Richter *b*-value, and it supplies a relative measure of the likelihood of large-magnitude and small-magnitude seismicity in the region. The correlation between seismic *b*-value, Bouguer gravity and heat flow data can be used for evaluating the nature of the crust and stress distribution in a specific region.

The cumulative number of earthquakes versus time in the study region is shown in Fig. 3. There is no significant change in the number of earthquakes as a function of time between 1970 and 1985 due to sparse station coverage. There is a minor change in the seismic activity after 1985 until 2000, while a significant change in the seismic activity is observed after 2000, and particularly after 2005, there has been a major change in seismic activity. The histogram for the eastern part of Turkey (Fig. 4a) between 1970 and 2010 indicates also an increase in the number of recorded events in the year 2005. However, the maximum increase in the number of earthquakes is observed in the year 2012. The magnitude scale in the catalogue ranges from 1.0 to 6.6 with an exponential decay in the frequency from lower to higher magnitudes. Figure 4b shows the histogram of magnitude distribution for the data set of the region. The magnitudes of most earthquakes are from 2.5 to 3.5, and a maximum is observed at $M_D = 2.8$.

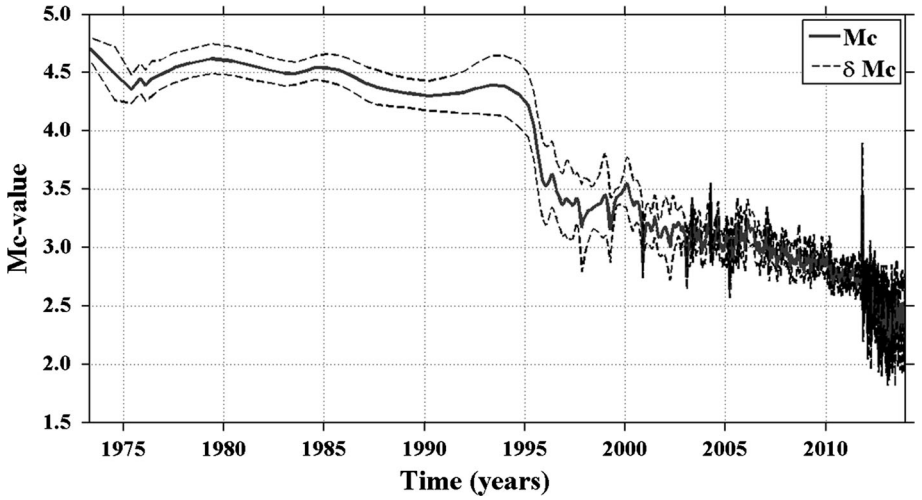

Fig. 5 Completeness magnitude, Mc, for the time period 1970–2014 for the Eastern Anatolia region. The standard deviation (δMc) of the completeness (*dashed lines*) is given. Mc is computed for overlapping samples, each containing 50 events

In order to calculate the seismic *b*-value from the frequency–magnitude relationship, the variation of Mc as a function of time is determined using a moving-window approach and is shown in Fig. 5. The Mc value is estimated for samples of 50 events/window by using all 30,461 earthquakes with $M_D \geq 1.0$. Mc has rather large values of 4.0–4.5 during 1975 and 1995, while it decreases to about 3.0 and 3.5 between 1995 and 2005. Then, it decreases to about 3.0 in the beginning of 2005, and for the latest events after 2005, Mc approaches the value of 2.5 which is consistent with the results of Öztürk and Bayrak (2012). It can be concluded that Mc generally shows non-stable values in the different periods.

The maximum-likelihood method is used to calculate the *b*-value from the Gutenberg–Richter (1944) relationship since this method yields a more robust estimate than the least-squares regression method (Aki 1965). Using the frequency–magnitude of earthquakes, the statistical behavior of seismic zones in the energy domain is described by the Gutenberg–Richter (G–R) law. Figure 6 shows the cumulative number of the earthquakes against the magnitude in the study region. With the Mc value assumed to be 2.8, the *b*-value is then calculated as 1.11 ± 0.08. The earthquakes are characterized by the *b*-value from 0.5 to 1.5 and more frequently around 1. It can be concluded that the earthquake catalogue is consistent with the general property of events. The magnitude–frequency distribution of the earthquakes is well represented by the G–R law with a *b*-value typically close to 1 (Fig. 6).

The regional distribution of *b*-value for the Eastern Anatolia region is presented in Fig. 7. The *b*-value is determined using a moving-window approach with maximum curvature method (MAXC) described in Woessner and Wiemer (2005). We used a total of 17,250 shallow earthquakes with $M_D \geq 2.8$, and *b*-value is estimated for 400 events/windows. A spatial grid of points with a distance of 0.1° is assumed. The *b*-value changes between 0.6 and 1.8. The highest *b*-values (>1.6) are located between the southeast of the Bozova fault and the southwest of the Karacadağ Extension Zone in the south of the study region. Also, the other large values changing between $\sim$1.2 and $\sim$1.5 are seen in the northwest part (between the Aşkale fault and the Erzurum fault, in the south and western

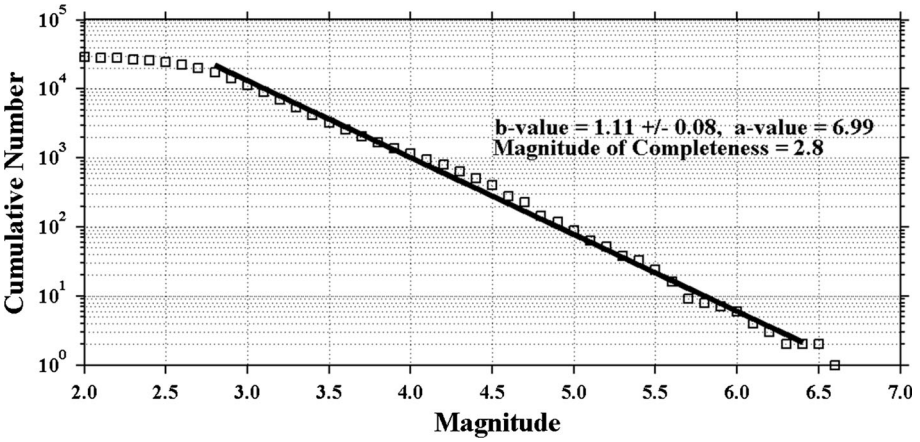

Fig. 6 Gutenberg–Richter relation and frequency–magnitude distributions of the earthquakes for the time period 1970–2014 for the Eastern Anatolia region. The *b*-value and its standard deviation, completeness magnitude as well as the *a*-value in the Gutenberg–Richter relation are given

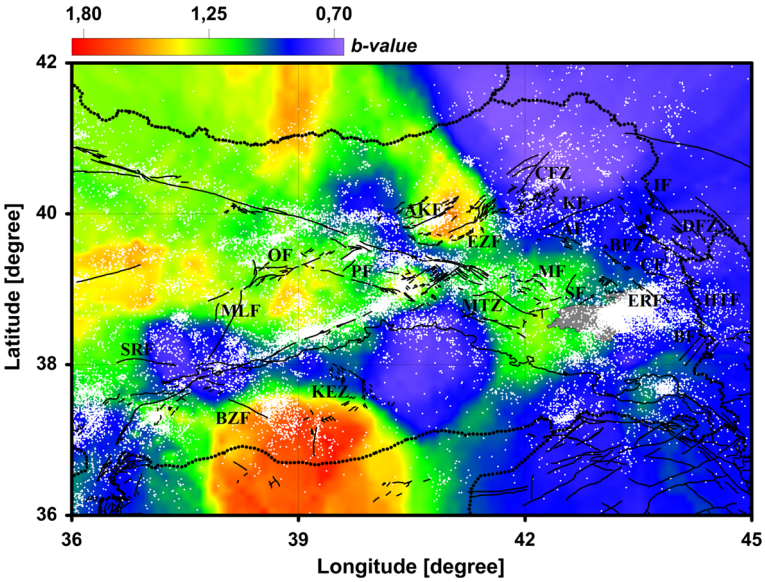

Fig. 7 Regional distribution of *b*-value for the Eastern Anatolia region. *White dots* represent the shallow earthquakes with depth less than 70 km and magnitude M_D larger than 2.8. Some faults given in the text (Sect. 4) are shown. Acronyms of the fault names are given in Fig. 1

part of Ovacık fault, in the Black Sea, between the Muş Thrust Zone and the Malazgirt fault, around the Malatya fault and the Pülümür fault). The lower *b*-values between 1.0 and 0.8 are found in a large area covering the rest of the study area, especially on the Eastern Anatolian Fault Zone and the Bitlis Thrust Zone. The lowest values (<0.7) are found in the other tectonic regions.

Changes in *b*-value versus depth are shown in Fig. 8, and these were analyzed in order to investigate the different behaviors of the individual zones. As shown in Table 1, detailed

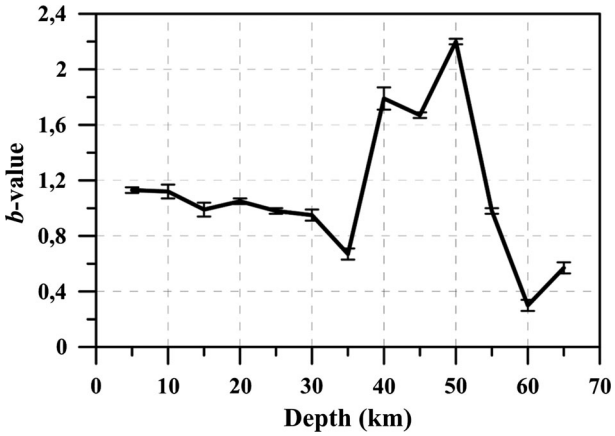

Fig. 8 Changes in *b*-value with depth for the Eastern Anatolia region

Table 1 Some parameters for different depths of earthquakes in the EAFZ

Depth (*D*) interval (km)	NOAE	NOEBE	MIOAE	MIOEBE	*Mc* value	*b*-Value	*a*-Value	POEBE (%)
$0.0 \leq D < 10.0$	20,660	12,041	1.0–6.6	2.8–5.5	2.8	1.13 ± 0.02	6.97	58.28
$5.0 \leq D < 15.0$	21,426	12,518	1.0–6.6	2.8–6.3	2.8	1.12 ± 0.05	6.89	58.44
$10.0 \leq D < 20.0$	6636	4055	1.0–6.2	2.7–6.2	2.7	0.99 ± 0.05	6.00	61.11
$15.0 \leq D < 25.0$	3343	1986	1.1–6.5	2.6–5.8	2.6	1.05 ± 0.02	6.03	59.37
$20.0 \leq D < 30.0$	2472	1669	1.0–6.5	2.9–5.9	2.6	0.98 ± 0.02	5.78	67.52
$25.0 \leq D < 35.0$	1597	801	1.0–6.0	2.9–6.0	2.9	0.95 ± 0.04	5.65	50.96
$30.0 \leq D < 40.0$	536	332	1.6–5.6	3.0–5.5	3.0	0.67 ± 0.04	4.53	61.94
$35.0 \leq D < 45.0$	109	49	1.9–5.1	4.3–5.1	4.3	1.79 ± 0.08	10.20	44.95
$40.0 \leq D < 50.0$	74	27	1.9–5.0	4.5–5.0	4.5	1.67 ± 0.02	11.40	36.49
$45.0 \leq D < 55.0$	69	26	2.0–5.0	4.5–5.0	4.5	2.20 ± 0.02	11.60	37.68
$50.0 \leq D < 60.0$	55	22	2.0–5.0	4.2–4.7	4.2	0.98 ± 0.02	7.57	40.00
$55.0 \leq D < 65.0$	31	26	2.4–5.1	2.9–4.7	2.9	0.30 ± 0.04	2.24	83.87
$60.0 \leq D < 70.0$	28	13	2.9–5.1	3.9–4.7	3.9	0.57 ± 0.04	2.88	46.43

NOAE number of all earthquakes, *NOEBE* number of earthquakes with *b*-value estimated, *MIOAE* magnitude interval of all earthquakes, *MIOEBE* magnitude interval of earthquakes with *b*-value estimated, *POEBE* percentage of earthquakes with *b*-value estimated

computations of *b*-values from the surface to a depth of 70 km are carried out for every 10-km-depth interval. An overlapping depth of 5 km (moving step) is used in order to ensure continuity of the data. Figure 8 shows that there is no significant change between 0 and 30 km, and the *b*-values in these depths vary between 1.0 and 1.1. There is a decrease in *b*-value (from 1.0 to 0.7) between 30 and 35 km depths. A strong increase from 0.7 to 2.2 is found between 35 and 50 km depths. The high *b*-values associated with the depth, coinciding with the lower crust, indicate that the study region is supported by a strong lithosphere (Khan and Chakraborty 2007). Magma chambers and the consequent normal stress reduction could have influenced the high *b*-values (Sanchez et al. 2004). On the

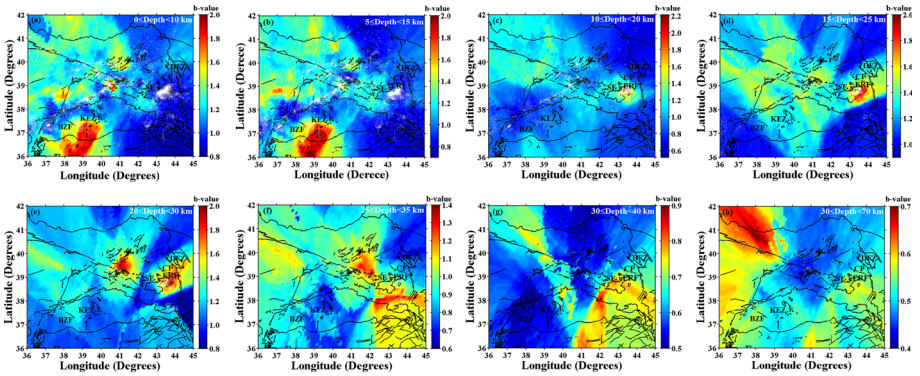

Fig. 9 Regional changes in *b*-value at different depths for the Eastern Anatolia region: **a** for 0–10 km, **b** 5–15 km, **c** 10–20 km, **d** 15–25 km, **e** 20–30 km, **f** 25–35 km, **g** 30–40 km and **h** 30–70 km. Some tectonic structures mentioned in the text (Sect. 4) are shown. Acronyms of the fault names are given in Fig. 1

contrary, a sharp decrease from 2.2 to 0.3 is also observed beyond this depth range ($D > 50$ km). In addition to these averaged *b*-values, regional variations of this parameter are plotted for different depths (Fig. 9).

As shown in Fig. 9a, b, *b*-values generally show a strong increasing and decreasing trend in the same regions for depths of 0–10 and 5–15 km. The largest *b*-values (>1.6) are observed between the southeast of Bozova fault and the southwest of the Karacadağ Extension Zone. The possible cause of the high *b*-value anomaly might be due to the release of magmatic gases caused by the pressure reduction at shallow depths. Groundwater interaction and the consequent normal stress decrease could also have affected the observed high *b*-values (Sanchez et al. 2004). Intermediate *b*-values (1.2–1.5) are found in the northwest part of the study region as also seen in Fig. 7. Such similarities are also observed in the other depths of 10–20, 15–25, 20–30 and 25–35 km. The regions with large and small *b*-values are the same in Fig. 9c, d, e, f.

It is widely accepted that the *b*-value increases with depth in volcanic regions and decreases with depth in non-volcanic regions (Wiemer et al. 1998; Katsumata 2006). In Fig. 9c, d, large *b*-values (>1.6) are observed between the Süphan and Erciş faults (around Lake Van). Also, the intermediate *b*-values are observed in the same areas. In Fig. 9e, the largest *b*-values are noted in the eastern part of the North Anatolian Fault Zone, in the regions including the Erciş, Çaldıran and Doğubeyazıt faults. The *b*-values greater than 1.1 in Fig. 9f are shown in the eastern part of the North Anatolian Fault Zone and southeast of the study region. However, there is a general decrease between 30–40 and 30–70 km. For these depths, the *b*-values are relatively small and vary from 0.4 to 0.9.

The gravity anomaly map (Fig. 10, colored surface), with a steep gradient decreasing from north to south of about −220 mGal, is mainly due to changes in rising crustal thickness. Zero gravity values mainly follow the Black Sea coastal line. The central part of the Bouguer anomaly map is dominated by a large negative anomaly lying in the E–W direction. The southeastern part of the Bouguer anomaly map is almost completely occupied with large negative anomalies owing to sedimentary basins of different ages (Maden et al. 2009).

The heat flow data (Fig. 10, contour lines) obtained from İlkışık (1995) indicate a close relation between high heat flow value and Tertiary and younger vulcanism. In the study

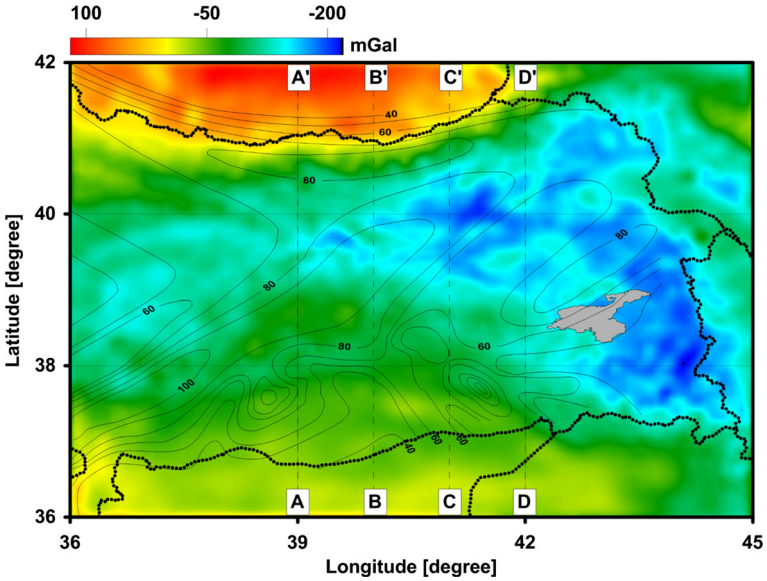

Fig. 10 Bouguer gravity anomaly (surface image) and surface heat flow (*contour lines*; from İlkışık 1995) maps for the Eastern Anatolia region. The heat flow contour interval is 10 m Wm^{-2}

area, the heat flow values vary from 40 to 100 mW m^{-2}. While the low heat flow values dominate in the Black Sea Basin, the Eastern Pontides orogenic belt shows relatively higher values. Along the southern Black Sea coast, the heat flow values increase markedly around the trench within a few kilometers to the south of the arc region. The highest heat flow values (105 mW m^{-2}) associated with extensive Neogene and Quaternary volcanic activity are observed in the Eastern Pontides orogenic belt. This sudden increase might be caused by a thicker continental crust (Maden 2013). The low and very low seismic Pn velocity zones in eastern Turkey, northwestern Iran and the Caucasus region may be associated with the latest stage of intense vulcanism during the Late Miocene (Al-Lazki et al. 2004). In the Black Sea, the heat flow contours follow the Black Sea shore line. The largest heat flow values are located on the East Anatolian Fault zone (100 mW m^{-2}), Eastern Pontides orogenic belt (80 mW m^{-2}) and north of the Lake Van (80 mW m^{-2}). Other high heat flow values are determined in the inner Eastern Anatolia region (89–99 mW m^{-2}) (Bektaş 2013) according to the steady-state geotherm model of Lachenbruch and Sass (1978). Thus, the high heat flow anomalies should be connected with tectonic zones that play an important role in the geodynamic evolution of the region. Two concentric circle-shaped negative heat flow anomalies are located in the southern part of the Anatolia near Mardin and Urfa, to the north of the Syrian border.

Comparisons of the surface heat flow data and the Bouguer gravity anomaly map (Fig. 10) with the *b*-value map (Fig. 7) give rise to some very interesting implications. The large negative gravity anomaly values located in the center of the region corresponding to low *b*-values mean that the crustal root is comparatively thicker and that a lower stress concentration exists (Fig. 10). The high *b*-values and positive gravity anomalies with a steep gradient toward the southern part of the region are associated with a thinner crust or a raised Moho causing higher stress concentration. The high *b*-values observed in the

eastern, western and southern areas, which are likely to be related to a magma chamber (Bektaş et al. 2007) or to crustal low-velocity zones as stated by Angus et al. (2006), are associated with comparatively lower Bouguer gravity anomalies. The East Anatolian plateau is thus supported not by thick crust, but by hot mantle as stated by Şengör et al. (2003). The low Bouguer gravity values and high *b*-values are consistent with a smaller concentration of stress, where energy has been intermittently dissipated through earthquakes. Mogi (1980) and Hirata (1987) noted that the *b*-value decreases before macroscopic failure caused by a decreasing external stress. Decrease in normal stress leads to the occurrence of relatively smaller earthquakes and thus increases the *b*-values (Sanchez et al. 2004). Scholz (1968) showed that *b*-value is inversely proportional to the stress applied to the rock sample.

A high *b*-value distribution has a correlation with high heat flow data (Fytikas and Kolios 1978). On the other hand, the areas showing low seismicity are occurring together with the higher heat flow values (Sanchez et al. 2004). The typical surface heat flow values are about 30–40 mW m^{-2} in fore-arc regions, more than 80–100 mW m^{-2} in the volcanic front and about 70–80 mW m^{-2} in back-arc regions (Hyndman and Lewis 1999). The highest heat flow values in the study region are related to the subduction zone (Fytikas 1980). The high *b*-values and high heat flow values located in the Eastern Pontide orogenic belt might be related to the magmatic activities beneath the volcanic chain associated with southward subduction of Tethys oceanic crust. On the other hand, Maden (2012) delineated that the Eurasia plate had moved from north to south under the Anatolia plate along the south Black Sea coast.

We selected four profiles; their locations are shown in Fig. 10, at the 39°, 40°, 41 and 42° latitudes in the NS direction. The *b*-values, gravity anomaly, surface heat flow data and earthquakes hypocenters with Moho and Conrad topography of the selected profiles are given in Fig. 10, 11, 12, 13 and 14a, b, c, d. We used $H = 32–0.08\Delta g$ (Wollard 1959) and $Hc = 18.6–0.031\Delta g$ (Demenitskaya 1967) to determine the Moho and Conrad depths of the region, respectively. In these formulas, Δg, H and Hc are gravity anomaly, the Moho and Conrad depths, respectively. These profiles depict a typical surface heat flow pattern over subduction zones through trench to the back-arc region. In our profiles, surface heat flow values are low in the trench and high in the arc and back-arc regions. Gravity values decrease from positive to negative values throughout the trench to island arc in Figs. 11, 12, 13 and 14. The Moho to surface distance is rather thick; earthquakes are relatively small beneath the volcanic chain where the higher surface heat flow values are observed. The common features of back-arc basins associated with subduction in relation to surface heat flow (Figs. 11, 12, 13 and 14) are summarized as: (1) less than normal heat flow over the zone from trench axis to volcanic zone; (2) high, but variable, heat flow over the volcanic zone or island arc; and (3) mean heat flow in back-arc extensional basins (Uyeda 1977).

The geodynamic evolution of the Eastern Black Sea Basin and the Pontides orogenic belt is still open to discussion due to the deficiency in systematical geological, geophysical and geochemical data. It is widely accepted that the Eastern Pontides orogenic belt was developed by northward subduction of Neotethys or Paleotethys oceanic lithosphere throughout the late Mesozoic, and the Black Sea Basin opened as a back-arc basin behind the Eastern Pontides magmatic arc (Şengör and Yılmaz 1981; Okay et al. 1994; Dilek et al. 2010). However, all of the results acquired from this study and prior paleomagnetic data promote the existence of the southward subduction model for the development of the Pontides during the late Mesozoic–Cenozoic. Dewey et al. (1973), Bektaş et al. (1999), Chorowicz et al. (1998), Eyuboglu et al. (2006), Eyuboglu (2010), Eyuboglu et al. (2011)

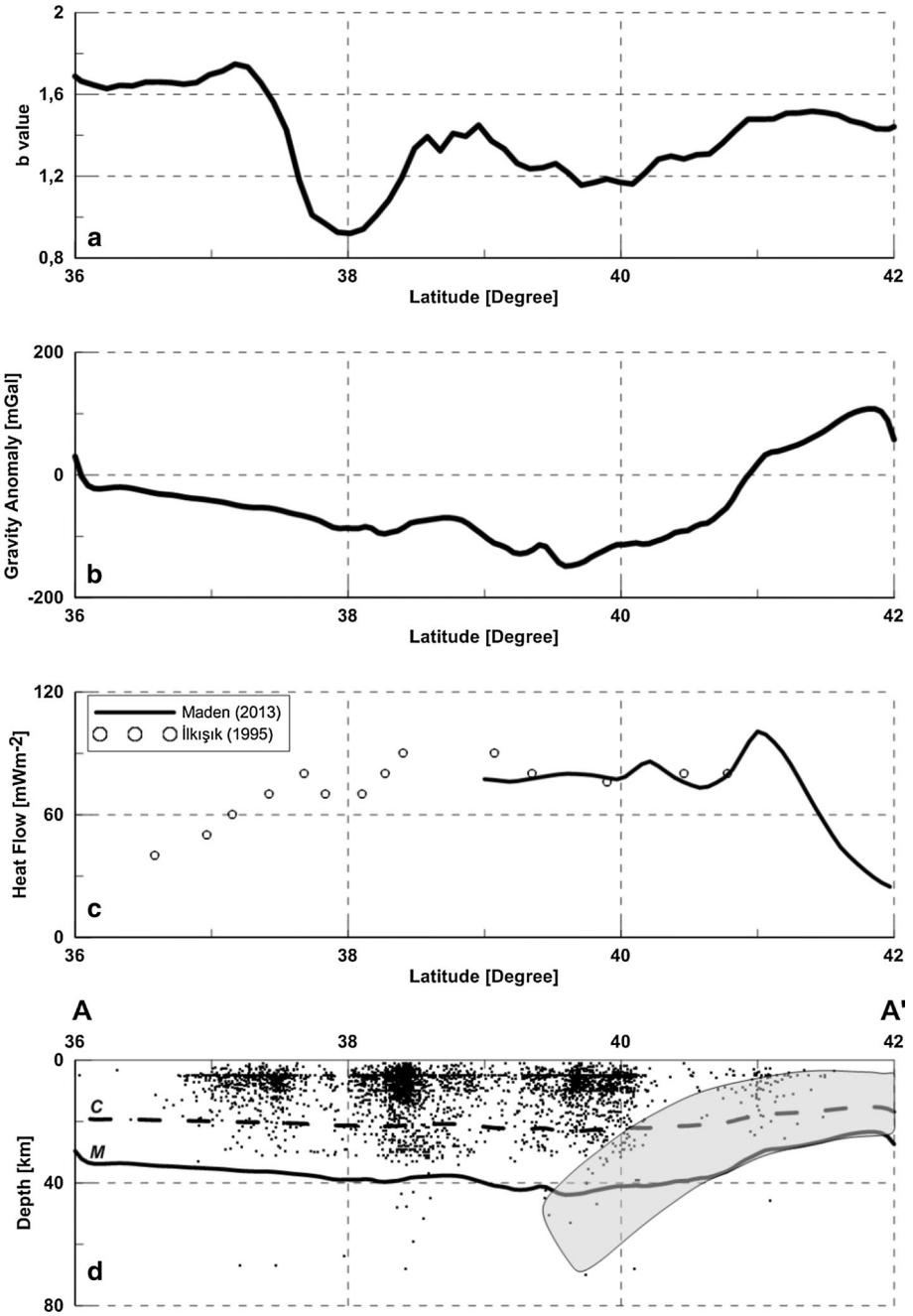

Fig. 11 **a** *b*-value, **b** Bouguer gravity anomaly, **c** surface heat flow density values determined from İlkışık (1995) (*open circles*) and Maden (2013) (*continuous lines*), and **d** distribution of earthquakes with depth along the 39° longitude. "C" stands for the Conrad interface, and "M" refers to the Moho discontinuity. The profile location is shown in Fig. 10

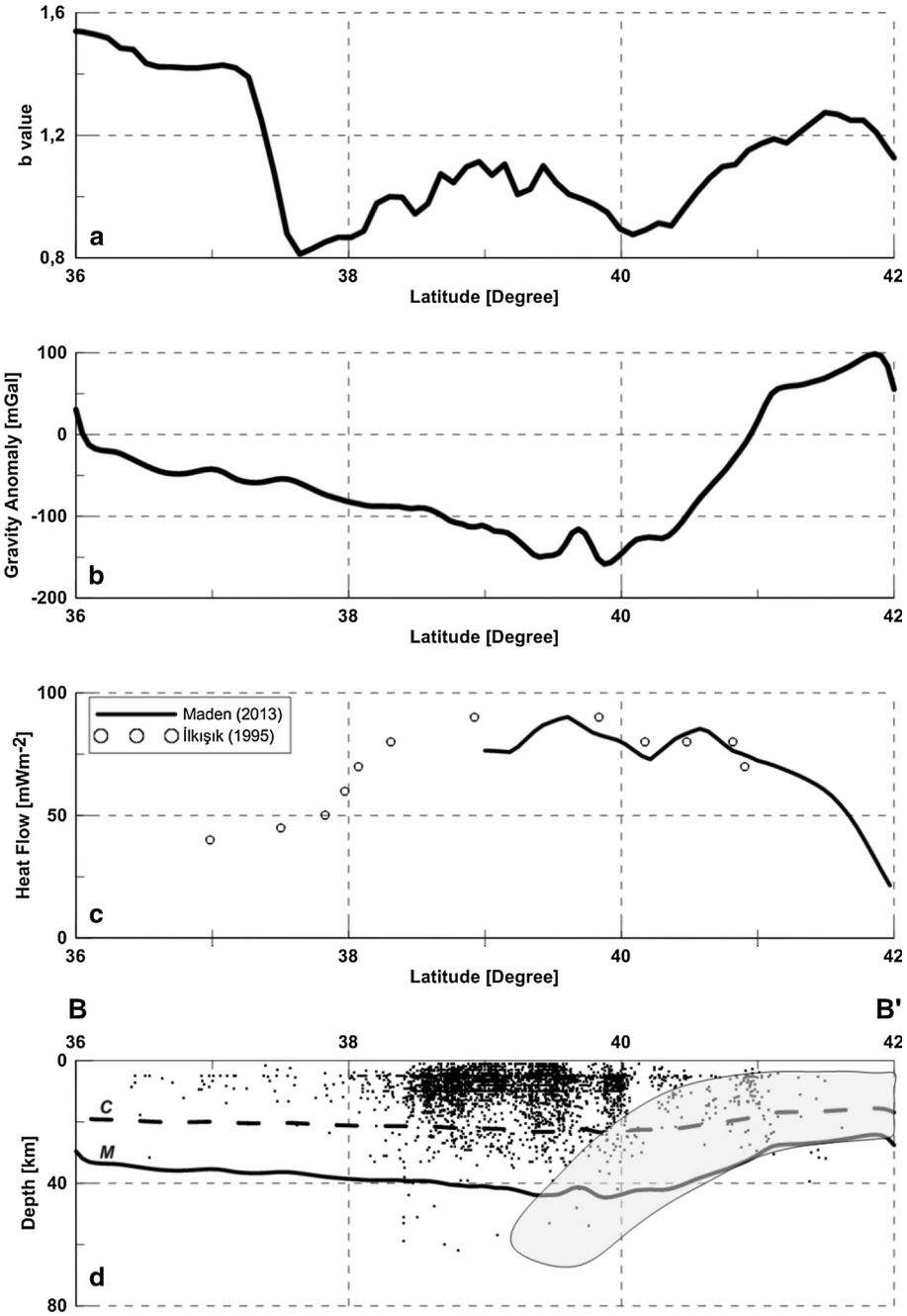

Fig. 12 **a** *b*-value, **b** Bouguer gravity anomaly, **c** surface heat flow density determined from İlkışık (1995) (*open circles*) and Maden (2013) (*continuous lines*), and **d** distribution of earthquake with depth along the 40° longitude. "C" stands for the Conrad interface, and "M" refers to the Moho discontinuity. The profile location is shown in Fig. 10

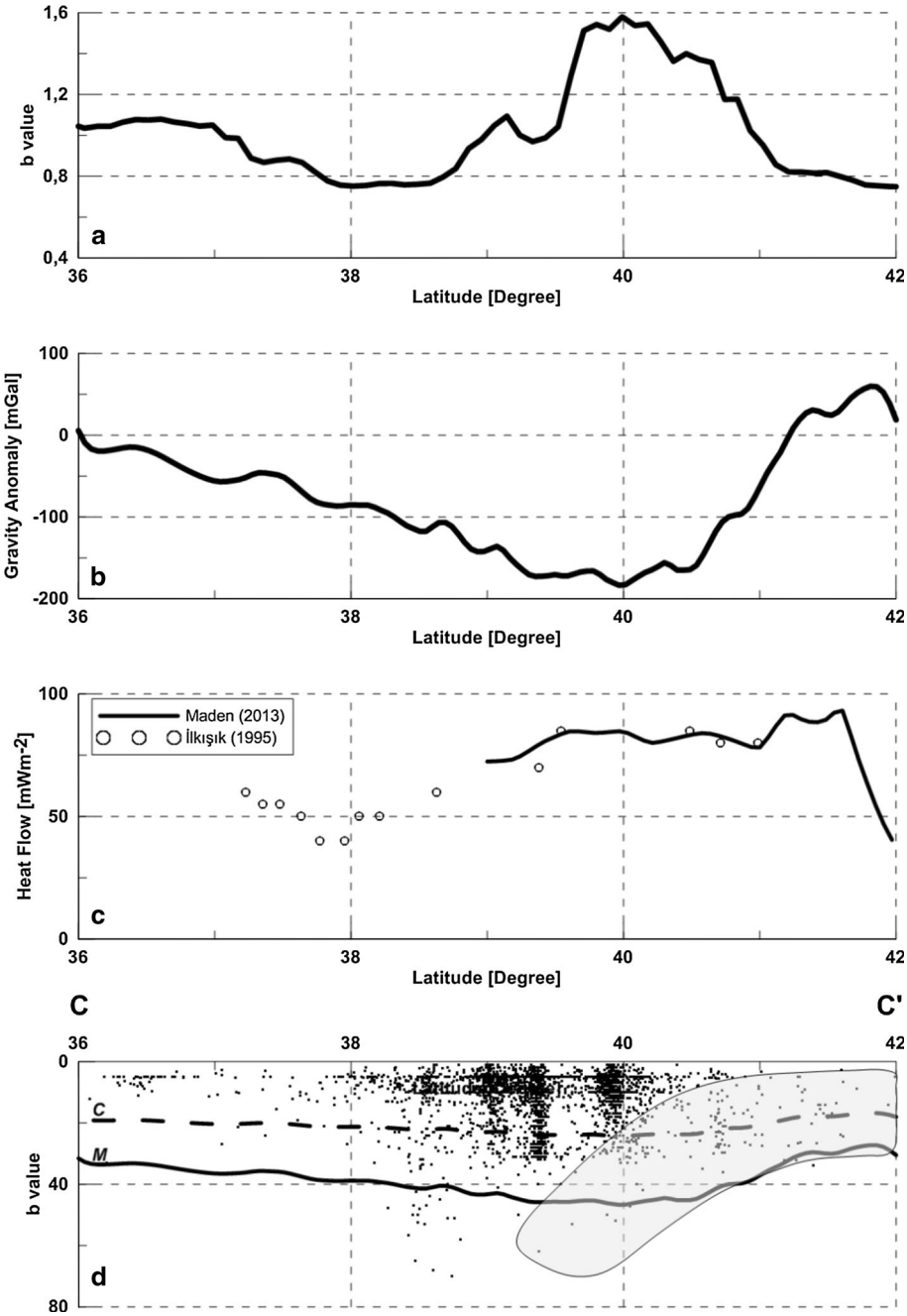

Fig. 13 **a** *b*-value, **b** Bouguer gravity anomaly, **c** surface heat flow density values determined from İlkışık (1995) (*open circles*) and Maden (2013) (*continuous lines*), and **d** distribution of earthquake with depth along the 41° longitude. "C" stands for the Conrad interface, and "M" refers to the Moho discontinuity. The profile location is shown in Fig. 10

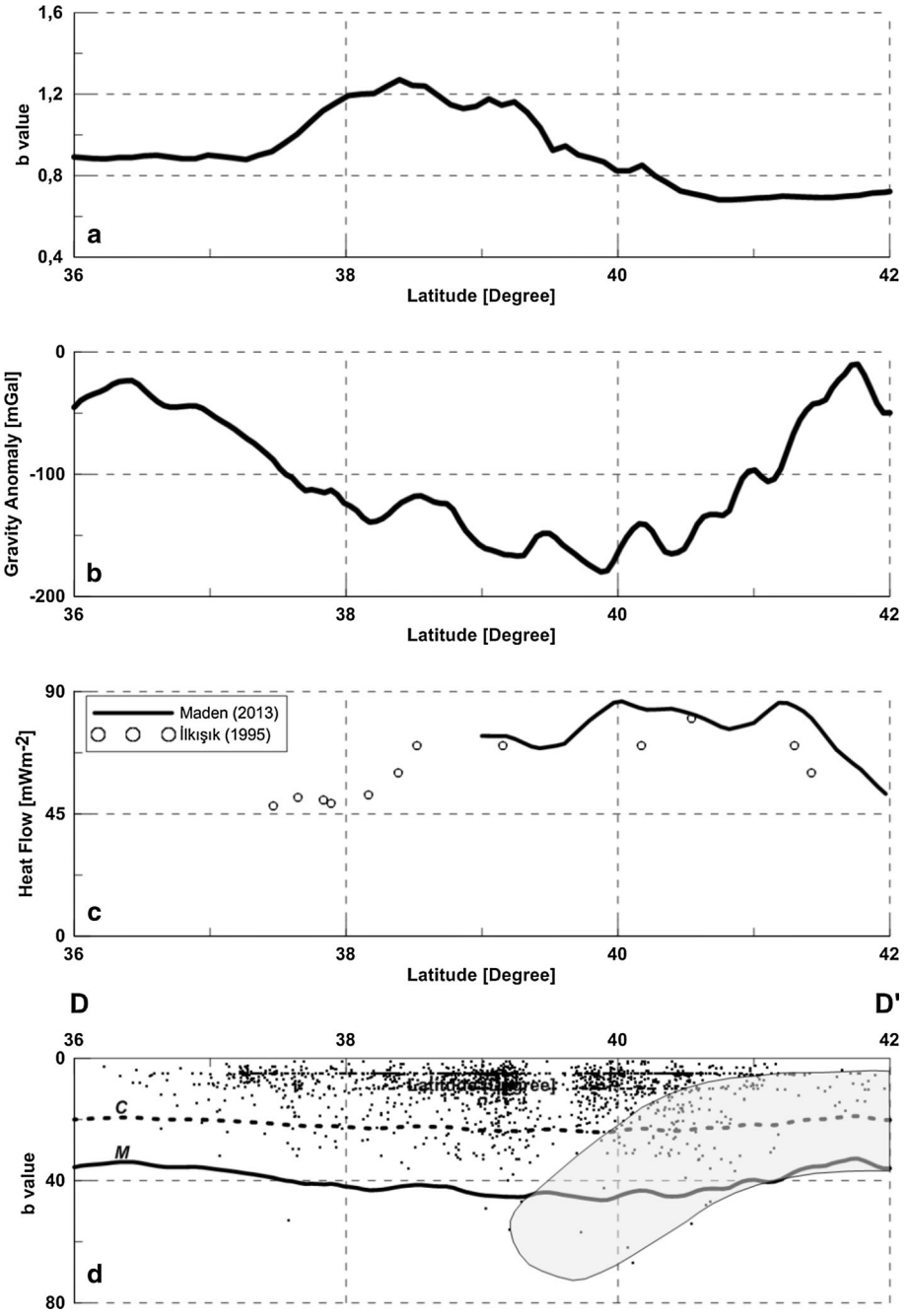

Fig. 14 **a** *b*-value, **b** Bouguer gravity anomaly, **c** surface heat flow density determined from İlkışık (1995) (*open circles*) and Maden (2013) (*continuous lines*), and **d** distribution of earthquake with depth along the 42° longitude. "C" stands for the Conrad interface, and "M" refers to the Moho discontinuity. The profile location is shown in Fig. 10

and Eyuboglu et al. (2013) proposed that the Eastern Pontides was built by the slab window mechanism in a southward subduction zone.

The paleomagnetic studies on the late Mesozoic–Cenozoic geodynamic improvement of the Eastern Mediterranean region point out that the Eastern Pontides orogenic belt was founded at 23° (Van der Voo 1968; Lauer 1981; Sarıbudak 1989), 25.5 ± 4.5° (Channell et al. 1996), 20.0 ± 2.5° (Çinku et al. 2010), 26.6° (Hisarlı 2011) north latitude in the Cretaceous. The present day position of the orogenic belt is established at between 39° and 42° latitude. This northward movement since the Cretaceous could be associated with southward subduction of the Tethys oceanic lithosphere.

The extensive young basaltic volcanism, regional travel time tomography and the broad-scale low-velocity regions determined from observations on seismic Pn and Sn phases, which underlie the East Anatolian high plateau, are interpreted to be hot and unstable mantle lid zones or deprived of mantle lithosphere. A region of no mantle lithosphere was interpreted as a subduction-accretion prism (East Anatolian Accretionary Complex of late Cretaceous to earliest Oligocene age) and slab breakoff beneath the prism (Pearce et al. 1990; Yilmaz 1993; Al-Lazki et al. 2003, Gök et al. 2003; Şengör et al. 2003; Al-Lazki et al. 2004).

Figure 15 shows the tectonic elements of the Black Sea Basin (Alptekin et al. 1986), and the Thrust faults occurred at the subduction zones (Barka and Reilinger 1997). Southward movement of the subducting plate and northward extension of the Black Sea increase the state of stress along the trench axis and decrease the *b*-value as seen in Figs. 11, 12, 13 and 14. These movements may load the stress energy to the fault systems. The 1968 Bartın earthquake ($M = 6.8$) occurred at the Thrust fault which lies parallel to the southern Black Sea coast. Thus, this margin can generate catastrophic earthquakes (Fig. 15).

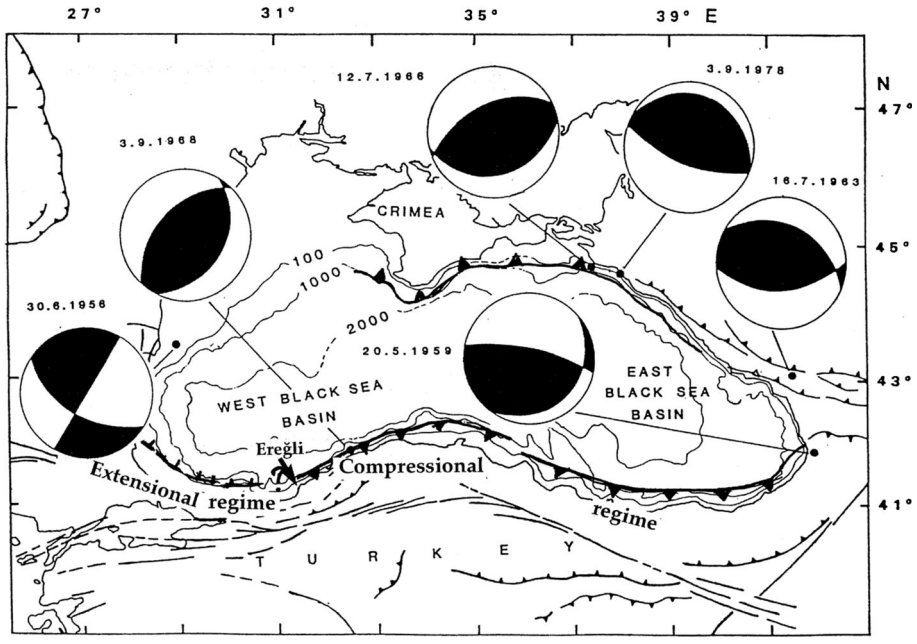

Fig. 15 Tectonics of the Black Sea Basin (Alptekin et al. 1986) and the Thrust faults occurring at the subduction zones of the Black Sea Basin (Barka and Reilinger 1997)

5 Conclusions

As a tool for tectonic implications, seismic *b*-value, Bouguer gravity and heat flow data in the Eastern Anatolia region of Turkey have been studied. Our analysis was carried out in the rectangular area limited by coordinates 36°N and 42°N in latitude and 36°N and 45°N in longitude. Earthquake catalogue consisting of 30,461 events at depths less than 70 km and magnitudes ranging from 1.0 to 6.6 was used. Bouguer gravity data were compiled from the General Directorate of Mineral Research and Exploration (MTA) and heat flow data from İlkışık (1995).

The Eastern Anatolia region has many major tectonic features with well-defined fault zones and an established history of seismic activity. From this aspect, a comparison of *b*-value, Bouguer gravity and heat flow data can have important tectonic implications for the region. Completeness magnitude is calculated as 2.8 and the *b*-value as 1.11 $\pm$ 0.08 for all earthquakes. This value is well represented by the Gutenberg–Richter law, typically close to 1. The *b*-value varies from 0.6 to 1.8. No important change in *b*-value is observed between the depths of 0 and 30 km. Strong fluctuations of the *b*-value 0.3–2.2 are seen between the depths of 35 and 60 km. Some properties such as magma chambers, stress reduction, groundwater interaction and volcanic activities can cause such kinds of fluctuations.

According to the spatial analysis of these three parameters, there are strong relationships among them. Large negative gravity values are related to small *b*-values, and the crustal structure is thick in these areas. Conversely, positive gravity values are compatible with high *b*-values, and these regions are interpreted as magma chamber or crustal low-velocity zones. It is suggested that large *b*-values and heat flow values may be compatible with the magmatic activities beneath the volcanic chain in the Eastern Pontide orogenic belt.

Considering the selected profiles, some conclusions could be reached: (1) The Moho discontinuity is fairly deep and earthquakes are relatively smaller beneath the volcanic chain where the high surface heat flow values are found, (2) the presence of the southward subduction model for the improvement of the Pontides throughout the late Mesozoic–Cenozoic might be reasonable, (3) hot and unstable mantle lid zones or a lithosphere deprived of mantle under the Eastern Anatolian high plateau could exist, (4) northward extension of the Black Sea and southward movement of the subduction plate strengthen the state of stress along the trench axis and reduce the *b*-value, and (5) these movements might stack the stress energy to the fault systems and so produce the catastrophic earthquakes in the Eastern Anatolia region.

Acknowledgments The authors would like to thank two anonymous reviewers for their useful and constructive suggestions which have improved this paper and also the Editor-in-Chief for his editorial suggestions. We would like to thank the General Directorate of the Mineral Research and Exploration (MTA) of Turkey for the provision of gravity data. We are also grateful to KOERI for providing earthquake database.

References

Aki K (1965) Maximum likelihood estimate of b in the formula log $N = a - bM$ and its confidence limits. Bull Earthq Res Inst Tokyo Univ 43:237–239

Al-Lazki AI, Sandvol E, Seber D, Turkelli N, Mohamad R, Barazangi M (2003) Tomographic Pn velocity and anisotropy structure beneath the Anatolian plateau (Eastern Turkey) and the surrounding regions. Geophys Res Lett 30:8040

Al-Lazki AI, Sandvol E, Seber D, Barazangi M, Turkelli N, Mohamad R (2004) Pn tomographic imaging of mantle lid velocity and anisotropy at the junction of the Arabian, Eurasian, and African plates. Geophys J Int 158:1024–1040

Alptekin Ö, Nabelek JL, Toksöz NM (1986) Source mechanism of the Bartın earthquake of September 3, 1968 in Northwestern Turkey: evidence for active thrust faulting at the Southern Black Sea margin. Tectonophysics 122:73–88

Angus DA, David C, Wilson E, Sandvol E (2006) Lithospheric structure of the Arabian and Eurasian collision zone in eastern Turkey from S-wave receiver functions. Geophys J Int 166:1335–1346

Barka A, Reilinger R (1997) Active tectonics of the Eastern Mediterranean region: deduced from GPS, neotectonic and seismicity data. Ann Geofis 40(3):587–610

Bayrak Y, Özturk S (2004) Spatial and temporal variations of the aftershock sequences of the 1999 İzmit and Duzce earthquake. Earth Planets Space 56:933–944

Bektaş Ö (2013) Thermal structure of the crust in Inner East Anatolia from aeromagnetic and gravity data. Phys Earth Planet Inter 221:27–37

Bektaş O, Şen C, Atıcı Y, Köprübaşı N (1999) Migration of the upper cretaceous subduction-related volcanism towards the back-arc basin of the Eastern Pontide magmatic arc (NE Turkey). Geol J 34:95–106

Bektaş Ö, Ravat D, Buyuksarac A, Bilim F, Ates A (2007) Regional geothermal characterisation of East Anatolia from aeromagnetic, heat flow and gravity data. Pure Appl Geophys 164:975–998

Bozkurt E (2001) Neotectonics of Turkey—a synthesis. Geodin Acta 14:3–30

Cao A, Gao SS (2002) Temporal variation of seismic b-value beneath north Eastern Japan island arc. Geophys Res Lett 29(48):1–3

Channell JET, Tuysuz O, Bektas O, Sengor AMC (1996) Jurassic-Cretaceous paleomagnetism and paleogeography of the Pontides (Turkey). Tectonics 115(1):201–212

Chorowicz J, Dhont D, Adıyaman Ö (1998) Black sea Pontides relationship: interpretation in terms of subduction. In: Third international turkish geology symposium, abstracts, Ankara, Turkey, METU, 258 p

Çinku MC, Ustaömer T, Hirt AM, Hisarli ZM, Heller F, Orbay N (2010) Southward migration of arc magmatism during latest Cretaceous associated with slab steepening, East Pontides, N Turkey: new paleomagnetic data from the Amasya region. Phys Earth Planet Inter 182:18–29

Demenitskaya RM (1967) Crust and Mantle of the Earth. Nedra, Moscow

Déverchère J, Petit C, Gileva N, Radziminovitch N, Melnikova V, San'kov V (2001) Depth distribution of earthquakes in the Baikal rift system and its implications for the rheology of the lithosphere. Geophys J Int 146:714–730

Dewey JF, Pitman WC, Ryan WBF, Bonin J (1973) Plate tectonics and the evolution of the Alpine system. Geol Soc Am Bull 84:3137–3180

Dilek Y, Imamverdiyev N, Altunkaynak S (2010) Geochemistry and tectonics of Cenozoic volcanism in the Lesser Caucasus (Azerbaijan) and the peri-Arabian region: collision-induced mantle dynamics and its magmatic fingerprint. Int Geol Rev 52(4–6):536–578

Eyuboglu Y (2010) Late cretaceous high-K volcanism in the Eastern pontide orogenic belt: implications for the geodynamic evolution of NE Turkey. Int Geol Rev 52:142–186

Eyuboglu Y, Bektaş O, Şeren A, Maden N, Özer R, Jacoby WR (2006) Three-directional extensional deformation and formation of the liassic rift basins in the Eastern Pontides (NE Turkey). Geol Carpath 57:337–346

Eyuboglu Y, Santosh M, Bektaş O, Ayhan S (2011) Arc magmatism as a window to plate kinematics and subduction polarity: example from the Eastern Pontides belt, NE Turkey. Geosci Front 2(1):49–56

Eyuboglu Y, Santosh M, Dudas FO, Akaryali E, Chung SL, Akdag K, Bektas O (2013) The nature of transition from adakitic to non-adakitic magmatism in a slab-window setting: a synthesis from the Eastern Pontides, NE Turkey. Geosci Front 4:353–375

Fagereng Å (2001) Frequency-size distribution of competent lenses in a block-in-matrix mélange: imposed length scales of brittle deformation? J Geophys Res 116:B05302. doi:10.1029/2010JB007775

Frohlich C, Davis S (1993) Teleseismic b-values: or, much ado about 1.0. J Geophys Res 98:631–644

Fytikas MD (1980) Geothermal exploitation in Greece. In: Strub AS ve Ungemach P (eds) 2nd International Seminar on the results of E. C. Geothermal Energy Research, Strasbourgh, pp 213–237, Reidel Publ., Dordrecht

Fytikas MD, Kolios NP (1978) Preliminary heatflow map of Greece. In: Cermak, Ryback (eds) Terrestial heat flow in Europe, p 270

Gök R, Sandvol E, Türkelli N, Seber D, Barazangi M (2003) Sn attenuation in the Anatolian and Iranian plateaus and surrounding regions. Geophys Res Lett 30:8042

Gök R, Pasyanos ME, Zor E (2007) Lithospheric structure of the continent–continent collision zone: Eastern Turkey. Geophys J Int 169:1079–1088
Gutenberg R, Richter CF (1944) Frequency of earthquakes in California. Bull Seism Soc Am 34:185–188
Hempton MR (1987) Constraints on Arabian plate motion and extensional history of the Red Sea. Tectonics 6:687–705
Hirata T (1987) Fractal structure of spatial distribution of microfracturing in rock. J Geophys Res 90:309–373
Hisarlı ZM (2011) New Paleomagnetic Constraints on the late Cretaceous and early Cenozoic tectonic history of the Eastern Pontides. J Geodyn 52:114–128
Hyndman RD, Lewis TJ (1999) Geophysical consequences of the Cordillera-Craton thermal transition in southwestern Canada. Tectonophysics 306:397–422
İlkışık OM (1992) Silica heat flow estimates and lithospheric temperature in Anatolia. In: Proceedings, XI congress of world hydrothermal organization, İstanbul, Mayıs 13–18, pp 92–104
İlkışık OM (1995) Regional heat flow in western Anatolia using silica temperature estimates from thermal springs. Tectonophysics 244:175–184
İlkışık OM, Gürer A, Tokgöz T, Kaya C (1997) Geoelectromagnetic and geothermic investigations in Ihlara Valley Geothermal Field. J Volcanol Geoth Res 78:297–308
Kalyoncuoglu UY, Elitok Ö, Dolmaz MN, Anadolu NC (2011) Geophysical and geological imprints of southern Neotethyan subduction between Cyprus and the Isparta Angle, SW Turkey. J Geodyn 52:70–82
Kalyoncuoglu UY, Elitok Ö, Dolmaz MN (2013) Tectonic implications of spatial variations of b-values and heat flow in the Aegean region. Mar Geophys Res 34:59–78
Katsumata K (2006) Imaging the high b-value anomalies within the subducting Pacific plate in the Hokkaido corner. Earth Planet Space 58:49–52
Khan PK (2005) Mapping of b-value beneath the Shillong Plateau. Gondwana Res 8(2):271–276
Khan PK, Chakraborty PP (2007) The seismic b-value and its correlation with Bouguer gravity anomaly over the Shillong Plateau area: tectonic implications. J Asian Earth Sci 29:136–147
Lachenbruch AH, Sass JH (1978) Models of an extending lithosphere and heat flow in the basin and range province. In: Smith RB, Eaton GP (eds) Cenozoic tectonics and regional geophysics of the Western Cordillera, vol 152, Geological Society of America Memoirs, pp 209–250
Lauer JP (1981) Orgine meridionale des Pontides d'apres de nouevaux resultats paleomagnetiques obtenus en Turqie. Bull Soc Geol Fr 23:619–624
Maden N (2012) Two-dimensional geothermal modeling along the Central Pontides magmatic arc (Northern Turkey). Surv Geophys 33:275–292
Maden N (2013) Geothermal structure of the Eastern Black Sea Basin and the Eastern Pontides Orogenic Belt: implications for subduction polarity of tethys oceanic lithosphere. Geosci Front 4:389–398
Maden N, Gelişli K, Bektaş O, Eyüboğlu Y (2009) Two-and-three-dimensional crust topography of the Eastern Pontides (NE Turkey). Turk J Earth Sci 18:225–238
Mogi K (1962) Magnitude-frequency relation for elastic shocks accompanying fractures of various materials and some related problems in earthquakes. Bull Earthq Res Inst Univ Tokyo 40:831–853
Mogi K (1980) Review of "Rock friction and earthquake prediction" edited by J.D. Byerlee and M. Wyss. Tectonophysics 65:378–379
Okay AI, Şengör AMC, Görür N (1994) Kinematic history of the opening of the Black Sea and its effect on the surrounding regions. Geology 22:267–270
Olsson R (1999) An estimation of the maximum b-value in the Gutenberg-Richter relation. Geodynamics 27:547–552
Öztürk S (2009) An application of the earthquake hazard and aftershock probability evaluation methods to Turkey Earthquakes, PhD Thesis, Karadeniz Technical University, Trabzon, Turkey (in Turkish with English abstract)
Öztürk S (2011) Characteristics of seismic activity in the Western, Central and Eastern Parts of the North Anatolian fault zone, Turkey: temporal and spatial analysis. Acta Geophys 59(2):209–238
Öztürk S, Bayrak Y (2012) Spatial variations of precursory seismic quiescence observed in recent years in the Eastern part of Turkey. Acta Geophys 60:92–118
Öztürk S, Çınar H, Bayrak Y, Karslı H, Daniel G (2008) Properties of the Aftershock Sequences of the 2003 Bingöl, MD = 6.4, (Turkey) Earthquake. Pure appl Geophys 165:349–371
Pearce JA, Bender JF, De Long SE, Kidd WSF, Low PJ, Guner Y, Saroglu F, Yilmaz Y, Moorbath S, Mitchell JG (1990) Genesis of collision volcanism in Eastern Anatolia, Turkey. J Volcanol Geotherm Res 44:189–229
Sanchez JJ, McNutt SR, Power JA, Wyss M (2004) Spatial variations in the frequency–magnitude distribution of earthquakes at Mount Pinatubo volcano. Bull Seismol Soc Am 94:430–438

Sarıbudak M (1989) New results and a paleomagnetic overview of the Pontides in Northern Turkey. Geophys J Int 99:521–531
Şaroğlu F, Emre O, Kuşcu I (1992) Active fault map of Turkey. General Directorate of Mineral Research and Exploration, Ankara, Turkey
Scholz CH (1968) The frequency-magnitude relationship of micro fracturing in rock and its relationship to earthquakes. Bull Seism Soc Am 58:399–415
Şengör AMC, Kidd WSF (1979) Post-collisional tectonics of the Turkish-Iranian plateau and a comparison with Tibet. Tectonophysics 55:361–376
Şengör AMC, Yılmaz Y (1981) Tethyan evolution of Turkey: a plate tectonic approach. Tectonophysics 75:181–241
Şengör AMC, Görür N, Şaroğlu F (1985) Strike-slip faulting and related basin formation in zones of tectonic escape: Turkey as a case study. In: Biddle KT, Christie-Blick N (eds) Strike-slip deformation, basin formation and sedimentation. Society of Economy, Palaeontology and Mineralogy Special Publication 37, pp 227–264
Şengör AMC, Özeren S, Zor E, Genç T (2003) East Anatolian high plateau as a mantle-supported, north-south shortened domal structure. Geophys Res Lett 30(24):8045
Sobiesiak M, Meyer U, Schmidt S, Götze Hj, Krawczyk CM (2007) Asperity generating upper crustal sources revealed by b value and isostatic residual anomaly grids in the area of Antofagasta, Chile. J Geophys Res 112:B12308
Tezcan AK (1995) Geothermal explorations and heat flow in Turkey. In: Gupta ML, Yamano M (eds) Terrestrial heat flow and geothermal energy in Asia. Science Publishers, Lebanon, New Hampshire, pp 23–42
Tezcan AK, Turgay MI (1989) Heat flow map of Turkey. General Directorate of Mineral Research and Exploration (MTA), Department of Geophysics Research, Ankara (in Turkish, unpublished)
Ulusay R, Tuncay E, Sönmez E, Gökçeoğlu C (2004) An attenuation relationship based on Turkish strong motion data and iso-acceleration map of Turkey. Eng Geol 74:264–291
Utsu T (1971) Aftershock and earthquake statistic (III): analyses of the distribution of earthquakes in magnitude, time and space with special consideration to clustering characteristics of earthquake occurrence (1). J Faculty Sci Hokkaido Univ Ser VII (Geophys.) 3:379–441
Uyeda S (1977) Some basic problems in the trench-arc-back arc system. In: Talwani M, Pitman WC III (eds) Island Arcs. Deep-sea Trenches and Back-arc Basins, Maurice Ewing Ser, 1, pp 1–14, AGU, Washington, DC
Van Der Voo R (1968) Jurassic, cretaceous and eocene pole positions from north Eastern Turkey. Tectonophysics 6:251–269
Wang JH (1988) b-values of shallow earthquakes in Taiwan. Seismol Soc Am Bull 66:1243–1254
Westeway R (1994) Present-day kinematics of the Middle East and Eastern Mediterranean. J Geophys Res 99:12071–12090
Wiemer S, Katsumata K (1999) Spatial variability of seismicity parameters in aftershock zones. J Geophys Res 104(B6):13135–13151
Wiemer S, Wyss M (2000) Minimum magnitude of completeness in earthquake catalogs: examples from Alaska, the Western United States, and Japan. Bull Seismol Soc Am 90:859–869
Wiemer S, McNutt SR, Wyss M (1998) Temporal and three-dimensional spatial analyses of the frequency–magnitude distribution near Long Valley Caldera, California. Geophys J Int 134:409–421
Woessner J, Wiemer S (2005) Assessing the quality of earthquake catalogues: estimating the magnitude of completeness and its uncertainty. Bull Seismol Soc Am 95(2):684–698. doi:10.1785/0120040007
Wollard GP (1959) Crustal structure from gravity and seismic soundings. J Geophys Res 64:1524–1544
Wong HK, Degens ET, Finckh P (1978) Structures in modern lake Van sediments as revealed by 3.5 KHz high resolution profiling. In: Degens ET, Kurtman F (eds) The Geology of Lake Van. Publication Institute of Mineral Research Exploration, vol 169, pp 11–19
Wyss M (1973) Towards a physical understanding of the earthquake frequency distribution. Geophys J R Astron Soc 31:341–359
Yilmaz Y (1993) New evidence and model on the evolution of the southeast Anatolian orogen. Geol Soc Am Bull 105:251–271
Yılmaz Y, Şaroğlu F, Güner Y (1987) Initiation of the neomagnetism in Eastern Anatolia. Tectonophysics 134:177–199